Lipid droplets fuels SARS-CoV-2 replication and inflammatory response

Suelen da Silva Gomes Dias[1#], Vinicius Cardoso Soares[1,2#], André C. Ferreira[1,3,4], Carolina Q. Sacramento[1,3], Natalia Fintelman-Rodrigues[1,3], Jairo R. Temerozo[5,6], Lívia Teixeira[1], Ester Barreto[1], Mayara Mattos[1,3], Caroline S. de Freitas[1,3], Isaclaudia G. Azevedo-Quintanilha[1], Pedro Paulo A. Manso[7], Eugenio D. Hottz[1,8], Camila R. R. Pão[1], Dumith C. Bou-Habib[5,6], Fernando A. Bozza[9,10], Thiago M. L. Souza[1,3], Patrícia T. Bozza[1]*

 # These authors contributed equally to this work

1- Laboratory of Immunopharmacology, Oswaldo Cruz Institute (FIOCRUZ), Rio de Janeiro, RJ, Brazil.

2- Program of Immunology and Inflammation, Federal University of Rio de Janeiro, UFRJ, Rio de Janeiro, RJ, Brazil.

3- National Institute for Science and Technology on Innovation on Diseases of Neglected Populations (INCT/IDNP), Center for Technological Development in Health (CDTS), Fiocruz, Rio de Janeiro, RJ, Brazil.

4- Universidade Iguaçu, Nova Iguaçu, RJ, Brazil.

5- Laboratory on Thymus Research, Oswaldo Cruz Institute (FIOCRUZ), Rio de Janeiro, RJ, Brazil.

6- National Institute for Science and Technology on Neuroimmunomodulation (INCT/NIM), Oswaldo Cruz Institute, Fiocruz, Rio de Janeiro, RJ, Brazil.

7- Laboratory of Patology, Oswaldo Cruz Institute (FIOCRUZ), Rio de Janeiro, RJ, Brazil.

8- Laboratory of Immunothrombosis, Department of Biochemistry, Federal University of Juiz de Fora (UFJF), Juiz de Fora, MG, Brazil;

9- National Institute of Infectology (INI), FIOCRUZ, Rio de Janeiro, Brazil.

10- D'Or Institute for Research and Education (IDOR), Rio de Janeiro, Brazil.

Keywords: SARS-CoV-2; COVID-19; Lipid metabolism; Lipid droplet; Pro-inflammatory cytokines.

*Corresponding author

Patrícia T. Bozza

pbozza@ioc.fiocruz.br or pbozza@gmail.com

Abstract

Viruses are obligate intracellular parasites that make use of the host metabolic machineries to meet their biosynthetic needs, identifying the host pathways essential for the virus replication may lead to potential targets for therapeutic intervention. The mechanisms and pathways explored by SARS-CoV-2 to support its replication within host cells are not fully known. Lipid droplets (LD) are organelles with major functions in lipid metabolism and energy homeostasis, and have multiple roles in infections and inflammation. Here we demonstrate that monocytes from COVID-19 patients have an increased LD accumulation compared to SARS-CoV-2 negative donors. *In vitro*, SARS-CoV-2 infection modulates pathways of lipid synthesis and uptake, as CD36, SREBP-1, PPARγ and DGAT-1 in human monocytes and triggered LD formation in different human cells. LDs were found in close apposition with SARS-CoV-2 proteins and double-stranded (ds)-RNA. The pharmacological modulation of LD formation by inhibition of DGAT-1 with A922500 significantly inhibited SARS-CoV-2 replication as well as reduced production of pro-inflammatory mediators. Taken together, we demonstrate the essential role of lipid metabolic reprograming and LD formation in SARS-CoV-2 replication and pathogenesis, opening new opportunities for therapeutic strategies to COVID-19.

Introduction

The coronavirus disease 2019 (COVID-19) caused by the novel severe acute respiratory syndrome-coronavirus 2 (SARS-CoV-2) has rapidly spread in a pandemic, representing an unprecedented health, social and economic threat worldwide (Lu et al., 2020; Wu et al., 2020). This newly emerged SARS-CoV-2 belongs to the *Betacoronavirus* genus of the subfamily *Orthocoronavirinae* in the *Coronaviridae* family. Like other Coronavirus, the SARS-CoV-2 is an enveloped non-segmented positive-sense RNA (+RNA) virus (Zhu et al., 2020), and its virus genome sequences have been shown to be similar to the already known SARS-CoV (Zhou et al., 2020b). Despite the similarity with other members of the *Betacoronavirus* genus, the pathogenesis of SARS-CoV-2 have unique properties that contribute to its severity and pandemic-scale spread. Therefore, it is necessary to understand how the virus interacts and manipulate host cell metabolism to better develop strategies to combat this new coronavirus pandemic.

Viruses are obligated intracellular pathogens and require host cell machinery to replicate (Chazal and Gerlier, 2003; Novoa et al., 2005; Takahashi and Suzuki, 2011). Viruses interact with several intracellular structures and have the ability to modulate cellular metabolism with benefit for viral replication (Abrantes et al., 2012; Syed et al., 2010; Zhang et al., 2017). Accumulate evidence point to major roles of lipid droplets (LD) for virus life cycle and pathogenesis, highlighting attention to its potential as target for drug development. Studies have demonstrated the interaction of viral proteins with proteins related to LD and the relevance of this organelle for viral replication as already demonstrated in several positive strand RNA (+ RNA) viruses such as *Flaviviridae* members, rotavirus and reovirus (Cheung et al., 2010; Coffey et al., 2006; Filipe and McLauchlan, 2015; Lyn et al., 2013; Samsa et al., 2009; Villareal et al., 2015). Accordingly, enzymes associated with lipid metabolism and pharmacological interventions that alter the formation of LDs and the synthesis of fatty acids reduces viral replication and assembly (Herker et al., 2010; Martín-Acebes et al., 2011; Villareal et al., 2015; Yang et al., 2008; Zhang et al., 2017). In addition, LD plays an important role in the infection pathogenesis and inflammatory processes (Herker and Ott, 2012; Pereira-Dutra et al., 2019).

Here we demonstrate major effects of SARS-CoV-2 to modulate lipid metabolism in human cells favoring increased de novo lipid synthesis and lipid remodeling, leading to increased LD accumulation in human cells. Increased LD accumulation is also observed in monocytes from COVID-19 patients when compared to healthy volunteers. Importantly, blocking LD biogenesis with the pharmacological inhibitor of DGAT-1 (A922500) blocks viral replication, pro-inflammatory cytokine production and cell death. Collectively, our results uncover mechanisms of viral manipulation of host cell lipid metabolism to allow SARS-CoV-2 replication and provide new ideas for antiviral strategy.

Results

SARS-CoV-2 infection upregulates lipid metabolism, increasing LD biogenesis in human cells.

Viruses have the ability to modulate cellular metabolism with benefits for viral replication. Several +RNA viruses, including various members of *Flaviviridae* family, as HCV (Boulant et al., 2007; Lyn et al., 2013) and DENV (Carvalho et al., 2012; Samsa et al., 2009) and also reovirus (Coffey et al., 2006), and poliovirus (Viktorova et al., 2018), modify the lipid metabolism in different cells and trigger LD formation, using these host organelles at different steps of their own replicative cycle,.

Here, we demonstrated increased LD accumulation in human monocytes from COVID-19 patients when compared with healthy volunteers (Fig. 1A and B). Likewise, we demonstrated that in vitro infection with SARS-CoV-2 at MOI of 0.01 triggers the increase of LDs in primary human monocytes within 24 hours (Fig. 1C and D), as well as in a lung epithelial human cell line (A549) (Supplementary Fig. 1A and B), and lung microvascular endothelial human cell line (HMVEC-L) (Supplementary Fig. 1C and D) after 48 hours of infection.

Lipid metabolism alterations in cells and plasma are emerging as major phenotypes during COVID-19 and SARS-CoV-2 infection (Shen et al., 2020). To gain insights on the mechanisms involved in LD formation, we evaluated the expression of the proteins associated with lipid metabolism important for lipid uptake and de novo lipid synthesis (Fig. 1E). As shown in figure 1E-G, SARS-CoV-2 infection induces the increase of pathways involved in lipid uptake as CD36, the major transcriptional factors involved in lipogenesis, PPARγ and SREBP-1, and DGAT-1 involved in triacylglycerol synthesis in human primary monocytes after 24 hours of infection.

Altogether, these data suggest that SARS-CoV-2 is able to modulate multiple pathways of lipid metabolism and remodeling, including immune cells from COVID-19 patients, culminating in new LD assembling in human cells.

Inhibition of LD formation lead to decreased viral replication and cell death in SARS-CoV-2 infected monocytes.

DGAT-1 is a key protein involved in the final step of triacylglycerol synthesis and thus is central to remodel and finish the biogenesis of LDs (Chitraju et al., 2017) . During HCV infection, DGAT-1 was shown to be required for LD biogenesis, and to control

HCV protein trafficking to LD (Camus et al., 2013). Consequently, DGAT-1 inhibition blocks HCV use of LD as replication platform and inhibits viral particle formation (Camus et al., 2013; Herker et al., 2010). To assess the importance of DGAT-1 to LD biogenesis during the SARS-CoV-2 infection, we pre-treated A549 cells with A922500, an inhibitor of the enzyme DGAT-1, for 2 hours at different concentrations and evaluated the LD biogenesis after 48 hours of SARS-CoV-2 infection. As shown in figure 2A and B, treatment with A922500 inhibited dose dependently the LD formation triggered by SARS-CoV-2 infection. Similarly, pre-treatment with A922500 also blocked LD induced by SARS-CoV-2 in monocytes (Fig. 2A and C).

Human monocytes infected with SARS-CoV-2 were shown to sustain genome viral replication, express higher level of pro-inflammatory cytokine and may undergo cell death (Codo et al., 2020). To gain insights on the functions of LDs in SARS-CoV-2 infection, LD biogenesis was inhibited by A922500, DGAT-1 inhibitor. Treatment with A922500 significantly reduced the viral load in human primary monocytes (Fig. 3A), suggesting a role for DGAT-1 and LD in SARS-CoV-2 replication.

It has already been demonstrated the capacity of the SARS-CoV-2 infection to induce cell death in monocytes, measured by the release of LDH in the supernatant (Fintelman-Rodrigues et al., 2020). Cell death after infection can occur due to cellular dysfunctions that lead to changes in cellular homeostasis caused by the virus replication and/or by the heightened inflammatory response. The cell death in human primary monocytes infected with SARS-CoV-2 was measured by the release of LDH into the supernatant, and also by the analysis of cell morphology observed in phase contrast. Our data showed that SARS-CoV-2 triggered increased LDH release in the supernatant and infected cells exhibited morphologic alterations with membrane rupture/damage in comparison with uninfected cells compatible with necrosis (Fig. 3B and C). The treatment with 10 μM of A922500 was able to inhibit SARS-CoV-2 induced cell death (Fig. 3B and C).

Lipid droplets are involved in SARS-CoV-2 heightened inflammatory response

Dysregulated immune response, with increased pro-inflammatory cytokine/chemokine production is observed during severe COVID-19 infection and associate with the outcome of the disease (Coperchini et al., 2020). We observed that primary human monocytes infected with SARS-CoV-2 exhibit increased production of leukotrienes, pro-inflammatory cytokines (IL-6, TNFα and IL-12) and chemokines (IL-8

and CXCL10) in comparison with uninfected monocytes (Fig. 3D, E and F). SARS-CoV-2 infection increased IL-10 and reduced IL-4 production in comparison with uninfected monocytes (Fig. 3F).

In leukocytes and other cells of the immune response, LDs are organelles with major functions in inflammatory mediator production and innate signaling. To evaluate if LDs contribute to SARS-CoV-2-induced inflammation, monocytes were pre-treated with A922500, and lipid mediators, cytokine and chemokines levels were measured 24 h after infection. It has been well established that LDs are organelles that compartmentalize eicosanoids synthesis machinery and are sites for eicosanoid formation (Bozza et al., 2011). Here, we demonstrated that SARS-CoV-2 infection increased LTB_4 and cysLT production in comparison with uninfected monocytes (Fig 3D). The pretreatment with DGAT-1 inhibitor A922500 reduced the LTB_4 and cysLT synthesis. This data demonstrate the importance of LD to the production of these pro-inflammatory lipid mediators. We observed that A922500 downregulated the chemokines IL-8 and CXCL10, and the pro-inflammatory cytokines IL-6, TNFα and IL-12 (Fig. 3E and F), but did not affect the anti-inflammatory cytokine IL-10 (Fig. 3G). Moreover, the inhibition of LDs may revert the pro-inflammatory profile by the increase of anti-inflammatory cytokine IL-4 (Fig. 3G).

Altogether, our data indicate that LDs have important functions in the modulation of inflammatory production in monocytes and suggest that LD inhibition may reduce the exaggerated inflammatory process caused by the cytokine storm.

Lipid droplets are sites for SARS-CoV-2 replication.

The up regulation of the lipid metabolism and LD biogenesis by the new SARS-CoV-2 suggest that the virus may explore host metabolism to favor it is replication using the LDs as a replication platform, as demonstrated for HCV (Boulant et al., 2007; Camus et al., 2013; Lee et al., 2019) and DENV (Samsa et al., 2009). To evaluate this, we used a VERO E6 cell line that has a highly replicative capacity.

For these experiments, we pre-treated the VERO cells with a range of concentrations of DGAT-1 inhibitor A922500 (0.1 - 50 μM) for 2 hours, followed by infection with SARS-CoV-2 (MOI 0.01) for 24 hours. The supernatant was used to perform a plaque assay. Here, we observed that A922500 significantly inhibited SARS-CoV-2 replication in a dose dependent manner with an IC50 of 3.78 μM (Fig. 4A and B).

To gain insights on the interaction of the SARS-CoV-2 with LDs we labeled the virus using serum from convalescent COVID-19 patient that exhibit high anti-SARS-CoV-2 titers. For that, we stained the LDs using a BODIPY probe and analyzed the co-localization between the virus and LDs by confocal microscopy. As shown in figure 4C, Intense immunoreactivity (red) was obtained in SARS-CoV-2 infected cells, whereas no labeling was observed in uninfected cells indicative of specific SARS-CoV-2 labeling with serum from convalescent COVID-19 (Fig. 4C). As observed for monocytes and lung cells, Vero E6 infected cells increased LD biogenesis (green). Then, we examined the spatial relationship between SARS-CoV-2 and LDs. Our confocal analysis show a close apposition of SARS-CoV-2 immunoreactivity with BODIPY-labeled LDs (red arrows) and also co-localization of viral protein(s) with BODIPY-labeled LDs (yellow; fuchsia arrows) in the infected cells (Fig. 4C-D).

Accumulating evidence indicate that host LDs play an important role in virus cycle, including as hubs for viral genome replication and viral particle assembly (Laufman et al., 2019; Lee et al., 2019; Miyanari et al., 2007; Samsa et al., 2009) . To access if LDs is associated with SARS-CoV-2 replication, we use a specific antibody for double stranded (ds)-RNA (J2 clone). As shown in figure 4E, we observed strong labeling of the ds-RNA in the cells infected with the SARS-CoV-2 compared to uninfected cell. Similar to labeling of the polyclonal serum from convalescent COVID-19, we observed close apposition and/or co-localization between BODIPY-labeled LD and ds-RNA (Fig. 4E and E`).

Collectively, our data suggest that SARS-CoV-2 uses LDs as a replication platform, and establish that pharmacological targeting of LD formation inhibit SARS-CoV-2 replication, emerging as a potential strategy for antiviral development.

Discussion

Most positive-strand RNA virus are able to modulate the host lipid metabolism and to highjack LDs to enhance their fitness and replication/particle assembling capacity (Herker and Ott, 2012; Pereira-Dutra et al., 2019). The pathways and mechanisms used may vary according to the virus and the host cell infected. The mechanisms and pathways explored by SARS-CoV-2 to support its replication within host cells are still largely unknown. Here we provided evidence that LDs participate at two levels of host pathogen interaction in SARS-CoV-2 infection: first, they are important players for virus replication; and second, they are central cell organelles in the amplification of inflammatory mediator production. First, we demonstrated that SARS-CoV-2 modulates pathways of lipid uptake and lipogenesis leading to increased LD accumulation in human host cells. We further showed that LDs are in close proximity with SARS-CoV-2 suggestive that LDs are recruited as part of replication compartment. Second, we showed that inhibition of DGAT-1 blocked LD biogenesis, and reduced virus replication, cell-death and pro-inflammatory mediator production.

LD biogenesis is a multi-mediated and highly coordinated cellular process that requires new lipid synthesis and/or lipid uptake and remodeling, but the molecular mechanisms involved in LD formation during inflammation and infection are still not completely understood. Here, we showed the increased expression of SREBP-1 and the nuclear receptor PPARγ after SARS-CoV-2 infection indicative of reprogramming of cells towards a lipogenic phenotype. Accordingly, increased expression of SREBP-1 has been reported after respiratory viruses including MERS-CoV, SARS-CoV, was shown important to the increase of the LD and the accumulation of the cholesterol during the infection and targeting the SREBP-associated lipid biosynthetic pathways were shown to have antiviral properties (Yuan et al., 2019). The transcription factor PPARγ is activated by lipid ligands and promotes the expression of proteins involved in lipid homeostasis and LD biogenesis, and has been implicated in infectious and non-infectious LD biogenesis in monocytes/macrophages (Almeida et al., 2014; Souza-Moreira et al., 2019). Based on this data we can suggest the importance of these two transcription factors during SARS-CoV-2 infection favoring the lipid synthesis and LD formation. One important gene up regulated by PPARγ is the membrane receptor CD36 (Cheng et al., 2016). CD36 plays an important role in the transport and uptake of long-chain fatty acids into cells and participates in pathological process, such as metabolic disorders and infections (Febbraio

et al., 2001). Previous reports showed that CD36 levels are increased in HCV and HIV-1 (Berre et al., 2013; Meroni et al., 2005) infection and it facilitates the viral attachment on host cell membrane contributing to viral replication (Cheng et al., 2016). Our results demonstrated that SARS-CoV-2 infection increase the CD36 expression in monocytes, suggesting the increase of lipids uptake can contribute to LD formation, observed after the infection.

Numerous studies established LDs as key organelles during +RNA viruses life cycle (Herker and Ott, 2012). Here, we observed strong labeling of the SARS-CoV-2 proteins and ds-RNA intimately associated to the LD and in some cases colocalizing with LD. This fact highly suggests that SARS-CoV-2 recruits LDs to replication compartments and could use it as building blocks to fuel replication. Indeed, recent studies have shed light on active mechanisms of LD recruitment to viral replication compartments with bi-directional content exchange and essential functions to replication and virus particle assembly (Laufman et al., 2019; Lee et al., 2019).

DGAT-1, the key enzyme for triacylglycerol synthesis, is critical for LD biogenesis and mediate viral protein trafficking to LD by HCV and other virus. Moreover, pharmacologically suppress of DGAT1 activity inhibits HCV replication at the assembly step (Camus et al., 2013; Herker et al., 2010). We observed DGAT-1 expression increases after SARS-CoV-2 infection and this enzyme can contribute for the LD remodeling in the host cells. Pharmacological inhibitors of lipid metabolism protein are able to modulate the LD formation. Therefore, we used the DGAT-1 inhibitor (A22500) during SARS-CoV-2 infection and we observed this treatment reduced the LD biogenesis in monocytes and A549 cells as well as decrease the viral load of SARS-CoV-2 in monocytes. Importantly, pharmacologically suppressing DGAT1 activity inhibited dose dependently SARS-CoV-2 infectious particle formation in VERO E6 cells with an IC50 of 3.78 μM. Thus, suggesting that DGAT-1 activity and LD formation are crucial to SARS-CoV-2 replication and assembly in these cells.

Dysregulated monocyte responses are pivotal in the uncontrolled production of cytokines during the infection with respiratory viruses, such as influenza A virus (Gao et al., 2013; Peschke et al., 1993). Dysregulated immune response with key involvement of monocytes, with increased pro-inflammatory cytokine/chemokine production is also observed during severe COVID-19 and is associated with the outcome of the disease (Coperchini et al., 2020; Zhou et al., 2020a). SARS-CoV-2 infection of human monocytes in vitro recapitulate most of the pattern of inflammatory mediator production associated

with COVID-19 severity, including the enhancement of the IL-6 and TNFα levels, and the consistent cell death, measured by LDH release (Fintelman-Rodrigues et al., 2020; Temerozo et al., 2020; Zhou et al., 2020a). We showed the SARS-CoV-2 infection was able to generate a large amount of inflammatory lipid mediators, and cytokine synthesis by monocytes. Blockage of DGAT-1 activity lead to inhibition of the LDs and significantly reduced leukotriene production and cytokine released by monocytes, suggesting an important role for LDs to control the inflammatory process, and consequently to prevent the cell death-related with the uncontrolled inflammatory process. This finding is in agreement with the well-established role of LDs in inflammation and innate immunity (Bozza and Viola, 2010; Pereira-Dutra et al., 2019). Therefore, our data support a role for LD in the heightened inflammatory production triggered by SARS-CoV-2 and conversely, inhibition of LD biogenesis by targeting DGAT1 activity may have beneficial effects in disease pathogenesis.

In summary, our data demonstrate that SARS-CoV-2 triggers reprograming of lipid metabolism in monocytes and other cells leading to accumulation of LDs favoring virus replication. The inhibition of LD biogenesis modulates the viral replication and the pro-inflammatory mediator production. Therefore, our data support the hypothesis that SARS-CoV-2 infection increases the expression of the lipid metabolism-related protein for their own benefit towards replication and fitness. Although, further studies are certainly necessary to better characterize the full mechanisms and importance of the LDs during the SARS-CoV-2 infection, our findings support major roles for LDs in SARS-CoV-2 life cycle and immune response. Moreover, the finding that the host lipid metabolism and LDs are required for SARS-CoV-2 replication suggests a potential strategy to interfere with SARS-CoV-2 replication by blocking the DGAT1 and other lipid metabolic pathway enzymes.

Acknowledgments

We thank the Hemotherapy Service from Hospital Clementino Fraga Filho (Federal University of Rio de Janeiro, Brazil) for providing buffy-coats. The authors thank the confocal imaging facility from the Rede de Plataformas Tecnológicas FIOCRUZ and Dr. Carmen Beatriz Wagner Giacoia Gripp for assessments related to BSL3 facility. This work was supported by grants from Inova program Fiocruz, Fundação de Amparo à Pesquisa do Estado do Rio de Janeiro (FAPERJ), Conselho Nacional de Desenvolvimento Científico e Tecnológico (CNPq) and Coordenação de Aperfeiçoamento de Pessoal de Nível Superior (CAPES) granted for Patrícia T. Bozza, Thiago Moreno L. Souza, Fernando A. Bozza.

Author Contribution.

Conceived the study: SSGD, VCS, FAB, TMLS, PTB; Designed the experiments: SSGD, VCS, TMLS; PTB; Performed the experiments: SSGD, VCS, ACF, CQS, NFR, JRT, LT, EB, MM, CSF, IGAQ, PPM, EH, CRRP; Analyzed the data: SSGD, VCS, DCBH, TMLS, PTB; Wrote the paper: SSGD, VCS, TMLS, PTB. All authors reviewed and approved the manuscript.

The authors declare no competing financial interests.

Figure Legends

Fig 1. SARS-CoV-2 infection modulates the lipid metabolism in human monocytes.

(A and C) LDs were captured by fluorescent microscopy after Oil Red O staining (Red) and nuclei stained with DAPI (Blue).

(A) Images representatives of monocytes from COVID-19 patients and health volunteers.

(C) Images representatives of human monocytes obtained from PBMC were infected by SARS-CoV-2 with MOI of 0.01 for 24 hours. Scale bar 20μm.

(B and D) LDs were evaluated by ImageJ software analysis by the measurement of the fluorescent area.

(E) Representative scheme of the increase of proteins associated with lipid metabolism by SARS-CoV-2 infection in monocyte can regulate the lipid droplet formation.

(F) Monocytes were infected by SARS-CoV-2 with MOI of 0.01 during 24h. Cell lysates were collected for the detection of CD36, PPAR-γ, SREBP-1, DGAT-1 by Western blotting. β-actin level were used for control of protein loading.

(G) Densitometry data set of each protein.

Data are expressed as mean ± SEM of five healthy volunteers (HV) for ex vivo experiments and three healthy donors for LDs staining and western blot. *p < 0.05 versus health volunteers or uninfected cells.

Fig 2. The A922500 inhibits lipid droplet biogenesis induced by SARS-CoV-2 in human pulmonary cells and monocytes.

Human pulmonary cell (A549 cell line) and monocytes were pre-treated with DGAT-1 inhibitor A922500 for 2 hours before the infection with SARS-CoV-2 at MOI of 0.01 during 24h in monocytes and 48h in A549 cell line.

(A) LDs were captured by fluorescent microscopy after Oil Red O staining (Red) and nuclei stained with DAPI (Blue). Scale bar 20μm.

(B and C) LDs were evaluated by ImageJ software analysis by the measurement of the fluorescent area of (B) A549 pre-treated with A922500 using different concentrations (0.1, 1 and 10μM) and (C) LDs from monocytes pre-treated with A922500 (10μM).

Data are expressed as mean ± SEM obtained in four independent experiments or donors. *p < 0.05 *versus* uninfected cells and #p < 0.05 *versus* A922500 treated cells.

Fig 3. Inhibitor A922500 decreases the pro-inflammatory profile and cell death induced by SARS-CoV-2 infection and reduces the viral load in human monocyte.

Monocytes were pre-treated with DGAT-1 inhibitor A922500 (10μM) for 2 hours before the infection with SARS-CoV-2 with MOI of 0.01 during 24h.

(A) Cell death was measured in the supernatant by LDH activity fold change in relation to the uninfected cell.

(B) Viral load by qPCR. Monocytes of each sample were counted for normalization.

(C) Images of phase contrast from monocytes. Scale bar 20μm.

(D-G) The inflammatory cytokines were measured in supernatants by ELISA (D) leukotrienes: CysLT and LTB_4, (E) chemokines: IL-8 and CXCL-10, (F) pro-inflammatory: IL-6, TNF-α and IL-12 and (G) anti-inflammatory cytokines: IL-10 and IL-4.

Data are expressed as mean ± SEM obtained in four independent donors. * p <0.05 *versus* uninfected cells and #p <0.05 *versus* A922500 treated cells.

Fig 4. Lipid droplets is necessary for SARS-CoV-2 replication in VERO E6.

VERO E6 were pre-treated with DGAT-1 inhibitor A922500 with different concentrations (0.1, 1, 10 and 50μM) for 2 hours before the infection with SARS-CoV-2 with MOI of 0.01 for 24h.

(A) Viral replication was determinate by Plaque assay.

(B) Representative Plaque assay.

(C-E) Immunofluorescence analyses of VERO E6 after SARS-CoV-2 infection with MOI of 0.01 for 48h. (C) The virus was detected by indirect immunofluorescence using convalescent donor serum (Red or white) or (E) the double strain RNA was detected by indirect immunofluorescence by J2 antibody (Red), the lipid droplets were stained with BODIPY 493/503 (Green) and nuclei stained with DAPI (Blue).

(C' and E') Representative zoom images.

Data are expressed of four independent experiments for SARS-CoV-2 replication and three for immunofluorescent analyse. #p <0.05 versus A922500 treated cells. Scale bar 20µm.

Fig S1. SARS-CoV-2 induces an increase of the LD biogenesis in different human pulmonary cell lines.

Human pulmonary cell lines were infected with SARS-CoV-2 at MOI of 0.01 for 48h.

(A and C) LDs were captured by fluorescent microscopy after Oil Red O staining (Red) and nuclei stained with DAPI (Blue).

(B and D) LDs were evaluated by ImageJ software analysis by the measurement of the fluorescent area.

Data are expressed of three independent experiments. *p <0.05 versus uninfected cells.

Scale bar 20µm.

Methodology

Cells, virus and reagents. Blood were obtained from COVID-19 RT-PCR-confirmed patients and health volunteers. Human monocytes were isolated from peripheral blood mononuclear cells (PBMCs) using density gradient centrifugation (Ficoll-Paque, GE Healthcare). The PBMC were resuspended in PBS containing 1 mM EDTA and 2 % fetal bovine serum (FBS; GIBCO) to the concentration of 10^8 cells/mL. The cells were incubated with anti-CD14 antibodies (1:10) for 10 min and magnetic beads-conjugates (1:20) for additional 10 min, followed by magnetic recovery of monocytes for 5 min. Recovered monocytes were resuspended in PBS containing 1 mM EDTA and 2 % FBS and subjected to two more rounds of selection in the magnet according to the manufacturer's instructions (Human CD14+ selection kit, Easy Sep; StemCell). The purity of monocyte preparations (>98% CD14+ cells) was confirmed through flow cytometry.

Human primary monocyte was obtained through plastic adherence of PBMCs. Briefly, PBMCs were isolated by Ficoll-Paque from peripheral blood or from buff-coat preparations of healthy donors. PBMCs (2×10^6) were plated onto 48-well plates in low glucose Dulbecco's modified Eagle's medium (DMEM; GIBCO). After 2 hours of the plaque, non-adherent cells were washed out and the remaining monocytes were maintained for 24 hours in DMEM containing 5% inactivated male human AB serum (HS; Merck) and 100 U/mL penicillin-streptomycin (P/S; GIBCO) at 37 °C in 5 % CO_2. The purity of human monocytes was above 90 %, as analyzed by flow cytometry analysis (FACScan; Becton Dickinson) using anti-CD3 (BD Biosciences) and anti-CD16 (Southern Biotech) monoclonal antibodies.

Human lung epithelial carcinoma line (A549 - ATCC/CCL-185) and African green monkey kidney (Vero subtype E6) were cultured in high glucose DMEM supplemented with 10% FBS and 100 U/mL P/S, and were incubated at 37 °C in 5 % CO_2.

Human lung microvascular endothelial line (HMVEC-L - LONZA/CC-2527) was maintained following the manufacturer's instructions. The cells were cultured in endothelial growth medium (EGM™-2MV BulletKit™, Clonetics) supplemented with 5 % fetal bovine serum (FBS, Clonetics) and cells were incubated at 37 °C and 5 % CO_2.

SARS-CoV-2 was originally isolated from nasopharyngeal swabs of confirmed case from Rio de Janeiro/Brazil (GenBank accession no. MT710714). The virus was amplified in Vero E6 cells in high glucose DMEM supplemented with 2% FBS, incubated at 37°C in 5% CO_2 during 2 to 4 days of infection. Virus titers were performed by the tissue culture infectious dose at 50% ($TCID_{50}$/mL) and the virus stocks kept in -80 °C freezers. According to WHO guidelines, all procedures involving virus culture were performed in biosafety level 3 (BSL3) multiuser facility.

Infections and virus titration. After 24h of cell plating, the SARS-CoV-2 infections were performed at MOI of 0.01 in all cells analyzed with or without pre-treatment for two hours with pharmacological inhibitor of the enzyme DGAT-1 (A922500 – Sigma CAS 959122-11-3). The Plaque-forming Assay were performed for virus titration, the VERO E6 were seeded in 24-well plates and infected the monolayer cells with different dilutions of the supernatant containing virus for 1h at 37°C. The cells were overlaid with high glucose DMEM containing 2% FSB and 2.4% carboxymethylcellulose. After 3 days, the cells were fixed with 10% formaldehyde in PBS for 3h. The monolayer cells were stained with 0.04% solution of crystal violet in 20% ethanol for 1h. The titer was calculated from the count of the plaques formed in the wells corresponding to the dilution and the unit expressed in plaque forming unit per mL (PFU/mL).

Lipid droplet staining. Human primary monocytes, A549 cell line, and HMVEC cell line were seeded in coverslips. The cells infected or not were fixed using 3.7% formaldehyde. In addition, after isolation, the monocytes from COVID-19 patients were fixed using 3.7% formaldehyde and adhered in coverslips through cytospin (500 x g for 5 min). The LDs were stained with 0.3% Oil Red O (diluted in 60% isopropanol) for 2 min at room temperature. The coverslips were mounted in slides using an antifade mounting medium (VECTASHIELD®). Nuclear recognition was based on DAPI staining (1 µg/mL) for 5 min. Fluorescence was analyzed by fluorescence microscopy with an 100x objective lens (Olympus, Tokyo, Japan). The numbers of LDs were automatically quantified by ImageJ software analysis from 15 aleatory fields.

Immunofluorescence staining. VERO E6 cells were seeded in coverslips and after 48h were fixed using 3.7% formaldehyde. Cells were rinsed three times with PBS containing 0.1 M CaCl2 and 1 M MgCl2 (PBS/CM) and then permeabilized with 0.1% Triton X-100

plus 0.2% BSA in PBS/CM for 10 min (PBS/CM/TB). Cells were stained with convalescent serum from a patient to identify with COVID-19 at 1:500 dilution for overnight, followed by a human anti-IgG-Alexa 546 at 1:1000 dilution for 1 h. The double-RNA was labeling by mouse monoclonal antibody J2 clone - Scicons (Schönborn et al., 1991) at 1:500 dilution for overnight, followed by a mouse anti-IgG-Dylight 550 at 1:1000 dilution for 1h. LDs were stained with BODIPY493/503 dye (dilution 1:5000 in water) for 5 min. The coverslips were mounted in slides using an antifade mounting medium (VECTASHIELD®). Nuclear recognition was based on DAPI staining (1 µg/mL) for 5 min. Fluorescence was analyzed by fluorescence microscopy with an 100x objective lens (Olympus, Tokyo, Japan) or Confocal Microscopy (Laser scanning microscopy LSM710 Meta, Zeiss).

SDS-page and Western blot. After 24h of SARS-CoV-2 infection, monocytes were harvested using ice-cold lysis buffer (1% Triton X-100, 2% SDS, 150 mM de NaCl, 10 mM de Hepes, 2 mM de EDTA plus protease inhibitor cocktail). Cell lysates were heated at 100 °C for 5 min in the presence of loading buffer (20% β-mercaptoethanol; 370 mM Tris base; 160 µM bromophenol blue; 6% glycerol; 16% SDS; pH 6.8). 20 µg of protein/sample were resolved by electrophoresis on 10% polyacrylamide SDS-PAGE. After electrophoresis, the separated proteins were transferred to nitrocellulose membranes and incubated in blocking buffer (5% nonfat milk, 50 mM Tris-HCl, 150 mM NaCl, and 0.1% Tween 20). Membranes were probed overnight with the following antibodies: anti-PPARγ (Santa Cruz Biotechnology, #SC-7196 - H100), anti-CD36 (Proteintech-18836-1-AP), anti-SREBP-1 (Ab-28481), anti-DGAT-1 (Santa Cruz Biotechnology, #SC-271934) and anti-β-actin (Sigma, #A1978). After the washing steps, they were incubated with IRDye - LICOR or HRP-conjugated secondary. All antibodies were diluted in blocking buffer. The detections were performed by Supersignal Chemiluminescence (GE Healthcare) or by fluorescence using the Odyssey system. The densitometries were analyzed using the software Image Studio Lite Ver 5.2.

Measurement of viral RNA loads. Supernatants from monocytes after 24h of SARS-CoV-2 infection were quantified for viral replication by detection of viral RNA. According to manufacter's protocols, the total RNA from each sample was extracted using QIAamp Viral RNA (Qiagen®). Quantitative RT-PCR was performed using QuantiTect Probe RT-PCR Kit (Quiagen®) in a StepOne™ Real-Time PCR System (Thermo Fisher Scientific). Amplifications were carried out containing 2× reaction mix

buffer, 50 µM of each primer, 10 µM of probe, and 5 µL of RNA template in 15 µL reaction mixtures. Primers, probes, and cycling conditions recommended by the Centers for Disease Control and Prevention (CDC) protocol were used to detect the SARS-CoV-2 (CDC, 2020). For virus quantification was employed the standard curve method. Cells of each sample were counted before the PCR analyses for normalization. The Ct values for this target were compared to those obtained to different cell amounts, 10^7 to 10^2, for calibration.

Measurements of inflammatory mediators and LDH activity. After 24 hours of SARS-CoV-2 infection, the monocyte supernatant with or without pre-treatment with A922500 in a concentration of 10 µM was obtained. Cytokines and chemokines were measured in the supernatant by ELISA following the manufacturer's instructions (Duo set, R&D). LTB_4 and cysLT were measured in the supernatant by EIA (Cayman Chemicals) following the manufacturer's instructions. Cell death was determined according to the activity of lactate dehydrogenase (LDH) in the culture supernatants using a CytoTox® Kit (Promega, USA) according to the manufacturer's instructions.

Ethics statement. Experimental procedures involving human cells from healthy donors were performed with samples obtained after written informed consent and were approved by the Institutional Review Board (IRB) of the Oswaldo Cruz Foundation/Fiocruz (Rio de Janeiro, RJ, Brazil) under the number 397-07. Experimental procedures involving human patient cells were performed with samples obtained after written informed consent from all participants or patients' representatives and were approved by the National Review Board approved the study protocol (CONEP 30650420.4.1001.0008).

Statistical analysis. Data are expressed as mean ± standard error of the mean (SEM) at least of three and maximum of five independent healthy donors. The paired two-tailed *t*-test was used to evaluate the significance of the two groups. Multiple comparisons among three or more groups were performed by one-way ANOVA followed by Tukey's multiple comparison test. p values < 0.05 were considered statistically significant when compared SARS-CoV-2 infection to the uninfected control (*) group or SARS-CoV-2 infection with A922500 treat group (#).

References

Abrantes, J.L., Alves, C.M., Costa, J., Almeida, F.C., Sola-Penna, M., Fontes, C.F., and Souza, T.M. (2012). Herpes simplex type 1 activates glycolysis through engagement of the enzyme 6-phosphofructo-1-kinase (PFK-1). Biochim Biophys Acta *1822*, 1198-1206.

Almeida, P.E., Roque, N.R., Magalhaes, K.G., Mattos, K.A., Teixeira, L., Maya-Monteiro, C., Almeida, C.J., Castro-Faria-Neto, H.C., Ryffel, B., Quesniaux, V.F.*, et al.* (2014). Differential TLR2 downstream signaling regulates lipid metabolism and cytokine production triggered by Mycobacterium bovis BCG infection. Biochim Biophys Acta *1841*, 97-107.

Berre, S., Gaudin, R., Cunha de Alencar, B., Desdouits, M., Chabaud, M., Naffakh, N., Rabaza-Gairi, M., Gobert, F.X., Jouve, M., and Benaroch, P. (2013). CD36-specific antibodies block release of HIV-1 from infected primary macrophages and its transmission to T cells. J Exp Med *210*, 2523-2538.

Boulant, S., Targett-Adams, P., and McLauchlan, J. (2007). Disrupting the association of hepatitis C virus core protein with lipid droplets correlates with a loss in production of infectious virus. J Gen Virol *88*, 2204-2213.

Bozza, P.T., Bakker-Abreu, I., Navarro-Xavier, R.A., and Bandeira-Melo, C. (2011). Lipid body function in eicosanoid synthesis: an update. Prostaglandins Leukot Essent Fatty Acids *85*, 205-213.

Bozza, P.T., and Viola, J.P. (2010). Lipid droplets in inflammation and cancer. Prostaglandins Leukot Essent Fatty Acids *82*, 243-250.

Camus, G., Herker, E., Modi, A.A., Haas, J.T., Ramage, H.R., Farese, R.V., and Ott, M. (2013). Diacylglycerol acyltransferase-1 localizes hepatitis C virus NS5A protein to lipid droplets and enhances NS5A interaction with the viral capsid core. J Biol Chem *288*, 9915-9923.

Carvalho, F.A., Carneiro, F.A., Martins, I.C., Assuncao-Miranda, I., Faustino, A.F., Pereira, R.M., Bozza, P.T., Castanho, M.A., Mohana-Borges, R., Da Poian, A.T.*, et al.* (2012). Dengue virus capsid protein binding to hepatic lipid droplets (LD) is potassium ion dependent and is mediated by LD surface proteins. J Virol *86*, 2096-2108.

CDC (2020). Centers for Disease Control and Prevention, Coronavirus Disease 2019 (COVID-19) (https://www.cdc.gov/coronavirus/2019-ncov/lab/rt-pcr-panel-primerprobes.html).

Chazal, N., and Gerlier, D. (2003). Virus entry, assembly, budding, and membrane rafts. Microbiol Mol Biol Rev *67*, 226-237, table of contents.

Cheng, J.J., Li, J.R., Huang, M.H., Ma, L.L., Wu, Z.Y., Jiang, C.C., Li, W.J., Li, Y.H., Han, Y.X., Li, H.*, et al.* (2016). CD36 is a co-receptor for hepatitis C virus E1 protein attachment. Sci Rep *6*, 21808.

Cheung, W., Gill, M., Esposito, A., Kaminski, C.F., Courousse, N., Chwetzoff, S., Trugnan, G., Keshavan, N., Lever, A., and Desselberger, U. (2010). Rotaviruses associate with cellular lipid droplet components to replicate in viroplasms, and compounds disrupting or blocking lipid droplets inhibit viroplasm formation and viral replication. J Virol *84*, 6782-6798.

Chitraju, C., Mejhert, N., Haas, J.T., Diaz-Ramirez, L.G., Grueter, C.A., Imbriglio, J.E., Pinto, S., Koliwad, S.K., Walther, T.C., and Farese, R.V. (2017). Triglyceride Synthesis by DGAT1 Protects Adipocytes from Lipid-Induced ER Stress during Lipolysis. Cell Metab *26*, 407-418.e403.

Codo, A.C., Davanzo, G.G., Monteiro, L.B., de Souza, G.F., Muraro, S.P., Virgilio-da-Silva, J.V., Prodonoff, J.S., Carregari, V.C., de Biagi Junior, C.A.O., Crunfli, F.*, et al.* (2020). Elevated Glucose Levels Favor SARS-CoV-2 Infection and Monocyte Response through a HIF-1α/Glycolysis-Dependent Axis. Cell Metab.

Coffey, C.M., Sheh, A., Kim, I.S., Chandran, K., Nibert, M.L., and Parker, J.S. (2006). Reovirus outer capsid protein micro1 induces apoptosis and associates with lipid droplets, endoplasmic reticulum, and mitochondria. J Virol *80*, 8422-8438.

Coperchini, F., Chiovato, L., Croce, L., Magri, F., and Rotondi, M. (2020). The cytokine storm in COVID-19: An overview of the involvement of the chemokine/chemokine-receptor system. Cytokine Growth Factor Rev *53*, 25-32.

568 Febbraio, M., Hajjar, D.P., and Silverstein, R.L. (2001). CD36: a class B scavenger receptor
569 involved in angiogenesis, atherosclerosis, inflammation, and lipid metabolism. J Clin Invest *108*,
570 785-791.
571 Filipe, A., and McLauchlan, J. (2015). Hepatitis C virus and lipid droplets: finding a niche. Trends
572 Mol Med *21*, 34-42.
573 Fintelman-Rodrigues, N., Sacramento, C.Q., Lima, C.R., da Silva, F.S., Ferreira, A.C., Mattos, M.,
574 de Freitas, C.S., Soares, V.C., Gomes Dias, S.d.S., Temerozo, J.R.*, et al.* (2020). Atazanavir inhibits
575 SARS-CoV-2 replication and pro-inflammatory cytokine production. bioRxiv,
576 2020.2004.2004.020925.
577 Gao, R., Bhatnagar, J., Blau, D.M., Greer, P., Rollin, D.C., Denison, A.M., Deleon-Carnes, M.,
578 Shieh, W.J., Sambhara, S., Tumpey, T.M.*, et al.* (2013). Cytokine and chemokine profiles in lung
579 tissues from fatal cases of 2009 pandemic influenza A (H1N1): role of the host immune response
580 in pathogenesis. Am J Pathol *183*, 1258-1268.
581 Herker, E., Harris, C., Hernandez, C., Carpentier, A., Kaehlcke, K., Rosenberg, A.R., Farese, R.V.,
582 and Ott, M. (2010). Efficient hepatitis C virus particle formation requires diacylglycerol
583 acyltransferase-1. Nat Med *16*, 1295-1298.
584 Herker, E., and Ott, M. (2012). Emerging role of lipid droplets in host/pathogen interactions. J
585 Biol Chem *287*, 2280-2287.
586 Laufman, O., Perrino, J., and Andino, R. (2019). Viral Generated Inter-Organelle Contacts
587 Redirect Lipid Flux for Genome Replication. Cell *178*, 275-289.e216.
588 Lee, J.Y., Cortese, M., Haselmann, U., Tabata, K., Romero-Brey, I., Funaya, C., Schieber, N.L.,
589 Qiang, Y., Bartenschlager, M., Kallis, S.*, et al.* (2019). Spatiotemporal Coupling of the Hepatitis C
590 Virus Replication Cycle by Creating a Lipid Droplet- Proximal Membranous Replication
591 Compartment. Cell Rep *27*, 3602-3617.e3605.
592 Lu, R., Zhao, X., Li, J., Niu, P., Yang, B., Wu, H., Wang, W., Song, H., Huang, B., Zhu, N.*, et al.*
593 (2020). Genomic characterisation and epidemiology of 2019 novel coronavirus: implications for
594 virus origins and receptor binding. Lancet *395*, 565-574.
595 Lyn, R.K., Hope, G., Sherratt, A.R., McLauchlan, J., and Pezacki, J.P. (2013). Bidirectional lipid
596 droplet velocities are controlled by differential binding strengths of HCV core DII protein. PLoS
597 One *8*, e78065.
598 Martín-Acebes, M.A., Blázquez, A.B., Jiménez de Oya, N., Escribano-Romero, E., and Saiz, J.C.
599 (2011). West Nile virus replication requires fatty acid synthesis but is independent on
600 phosphatidylinositol-4-phosphate lipids. PLoS One *6*, e24970.
601 Meroni, L., Giacomet, V., Morelli, P., Erba, P., Galazzi, M., Riva, A., Viganò, A., and Galli, M.
602 (2005). Increased CD36 expression in vertically human immunodeficiency virus-infected children
603 unrelated to antiretroviral therapy. Pediatr Infect Dis J *24*, 576-577.
604 Miyanari, Y., Atsuzawa, K., Usuda, N., Watashi, K., Hishiki, T., Zayas, M., Bartenschlager, R.,
605 Wakita, T., Hijikata, M., and Shimotohno, K. (2007). The lipid droplet is an important organelle
606 for hepatitis C virus production. Nat Cell Biol *9*, 1089-1097.
607 Novoa, R.R., Calderita, G., Arranz, R., Fontana, J., Granzow, H., and Risco, C. (2005). Virus
608 factories: associations of cell organelles for viral replication and morphogenesis. Biol Cell *97*,
609 147-172.
610 Pereira-Dutra, F.S., Teixeira, L., de Souza Costa, M.F., and Bozza, P.T. (2019). Fat, fight, and
611 beyond: The multiple roles of lipid droplets in infections and inflammation. J Leukoc Biol *106*,
612 563-580.
613 Peschke, T., Bender, A., Nain, M., and Gemsa, D. (1993). Role of macrophage cytokines in
614 influenza A virus infections. Immunobiology *189*, 340-355.
615 Samsa, M.M., Mondotte, J.A., Iglesias, N.G., Assuncao-Miranda, I., Barbosa-Lima, G., Da Poian,
616 A.T., Bozza, P.T., and Gamarnik, A.V. (2009). Dengue virus capsid protein usurps lipid droplets
617 for viral particle formation. PLoS Pathog *5*, e1000632.

618 Schönborn, J., Oberstrass, J., Breyel, E., Tittgen, J., Schumacher, J., and Lukacs, N. (1991).
619 Monoclonal antibodies to double-stranded RNA as probes of RNA structure in crude nucleic acid
620 extracts. Nucleic Acids Res *19*, 2993-3000.
621 Shen, B., Yi, X., Sun, Y., Bi, X., Du, J., Zhang, C., Quan, S., Zhang, F., Sun, R., Qian, L.*, et al.* (2020).
622 Proteomic and Metabolomic Characterization of COVID-19 Patient Sera. Cell *182*, 59-72.e15.
623 Souza-Moreira, L., Soares, V.C., Dias, S.D.S.G., and Bozza, P.T. (2019). Adipose-derived
624 Mesenchymal Stromal Cells Modulate Lipid Metabolism and Lipid Droplet Biogenesis via
625 AKT/mTOR -PPARγ Signalling in Macrophages. Sci Rep *9*, 20304.
626 Syed, G.H., Amako, Y., and Siddiqui, A. (2010). Hepatitis C virus hijacks host lipid metabolism.
627 Trends Endocrinol Metab *21*, 33-40.
628 Takahashi, T., and Suzuki, T. (2011). Function of membrane rafts in viral lifecycles and host
629 cellular response. Biochem Res Int *2011*, 245090.
630 Temerozo, J.R., Sacramento, C.Q., Fintelman-Rodrigues, N., Pão, C.R.R., de Freitas, C.S., da Silva
631 Gomes Dias, S., Ferreira, A.C., Mattos, M., Soares, V.C., Teixeira, L.*, et al.* (2020). The
632 neuropeptides VIP and PACAP inhibit SARS-CoV-2 replication in monocytes and lung epithelial
633 cells, decrease the production of proinflammatory cytokines, and VIP levels are associated with
634 survival in severe Covid-19 patients. bioRxiv, 2020.2007.2025.220806.
635 Viktorova, E.G., Nchoutmboube, J.A., Ford-Siltz, L.A., Iverson, E., and Belov, G.A. (2018).
636 Phospholipid synthesis fueled by lipid droplets drives the structural development of poliovirus
637 replication organelles. PLoS Pathog *14*, e1007280.
638 Villareal, V.A., Rodgers, M.A., Costello, D.A., and Yang, P.L. (2015). Targeting host lipid synthesis
639 and metabolism to inhibit dengue and hepatitis C viruses. Antiviral Res *124*, 110-121.
640 Wu, F., Zhao, S., Yu, B., Chen, Y.M., Wang, W., Song, Z.G., Hu, Y., Tao, Z.W., Tian, J.H., Pei, Y.Y.*,*
641 *et al.* (2020). A new coronavirus associated with human respiratory disease in China. Nature *579*,
642 265-269.
643 Yang, W., Hood, B.L., Chadwick, S.L., Liu, S., Watkins, S.C., Luo, G., Conrads, T.P., and Wang, T.
644 (2008). Fatty acid synthase is up-regulated during hepatitis C virus infection and regulates
645 hepatitis C virus entry and production. Hepatology *48*, 1396-1403.
646 Yuan, S., Chu, H., Chan, J.F., Ye, Z.W., Wen, L., Yan, B., Lai, P.M., Tee, K.M., Huang, J., Chen, D.*,*
647 *et al.* (2019). SREBP-dependent lipidomic reprogramming as a broad-spectrum antiviral target.
648 Nat Commun *10*, 120.
649 Zhang, J., Lan, Y., and Sanyal, S. (2017). Modulation of Lipid Droplet Metabolism-A Potential
650 Target for Therapeutic Intervention in. Front Microbiol *8*, 2286.
651 Zhou, F., Yu, T., Du, R., Fan, G., Liu, Y., Liu, Z., Xiang, J., Wang, Y., Song, B., Gu, X.*, et al.* (2020a).
652 Clinical course and risk factors for mortality of adult inpatients with COVID-19 in Wuhan, China:
653 a retrospective cohort study. Lancet *395*, 1054-1062.
654 Zhou, P., Yang, X.L., Wang, X.G., Hu, B., Zhang, L., Zhang, W., Si, H.R., Zhu, Y., Li, B., Huang, C.L.*,*
655 *et al.* (2020b). A pneumonia outbreak associated with a new coronavirus of probable bat origin.
656 Nature *579*, 270-273.
657 Zhu, N., Zhang, D., Wang, W., Li, X., Yang, B., Song, J., Zhao, X., Huang, B., Shi, W., Lu, R.*, et al.*
658 (2020). A Novel Coronavirus from Patients with Pneumonia in China, 2019. N Engl J Med *382*,
659 727-733.

660

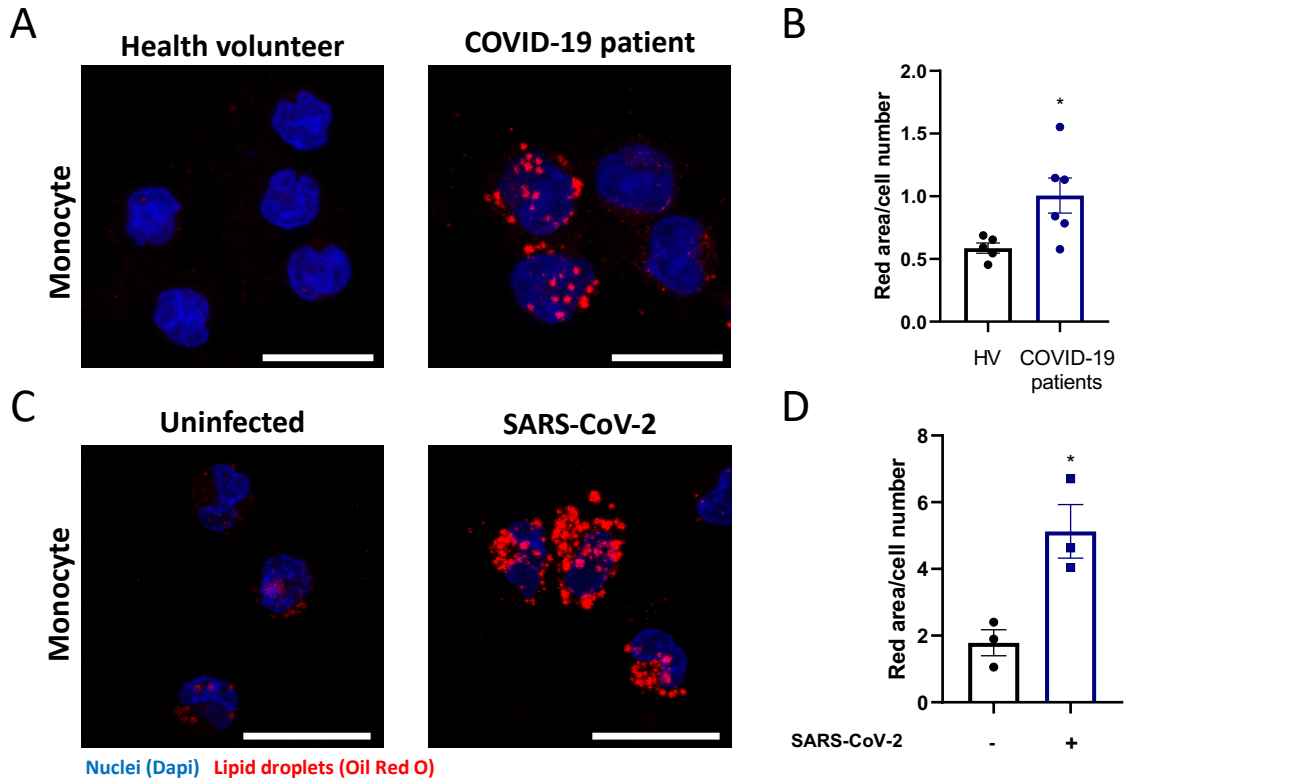
A
Health volunteer
COVID-19 patient
Monocyte
B
Red area/cell number
2.0
1.5
1.0
0.5
0.0
*
HV
COVID-19 patients
C
Uninfected
SARS-CoV-2
Monocyte
D
Red area/cell number
8
6
4
2
0
*
SARS-CoV-2
-
+
Nuclei (Dapi)
Lipid droplets (Oil Red O)

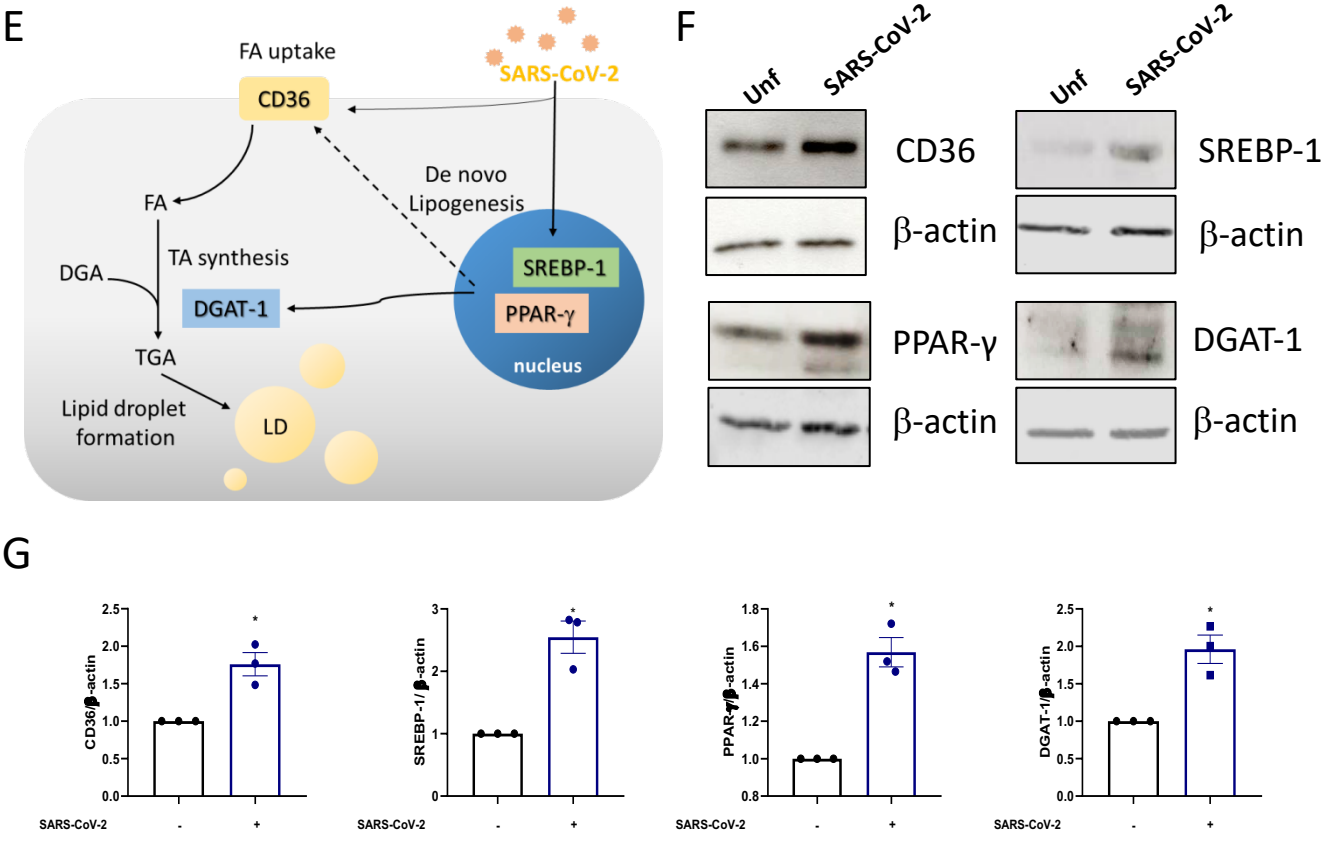
E
FA uptake
SARS-CoV-2
CD36
FA
De novo Lipogenesis
DGA
TA synthesis
SREBP-1
DGAT-1
PPAR-γ
TGA
nucleus
Lipid droplet formation
LD
F
Unf
SARS-CoV-2
CD36
β-actin
SREBP-1
β-actin
PPAR-γ
β-actin
DGAT-1
β-actin

G
CD36/β-actin
SREBP-1/β-actin
PPAR-γ/β-actin
DGAT-1/β-actin
SARS-CoV-2
-
+

Figure 1

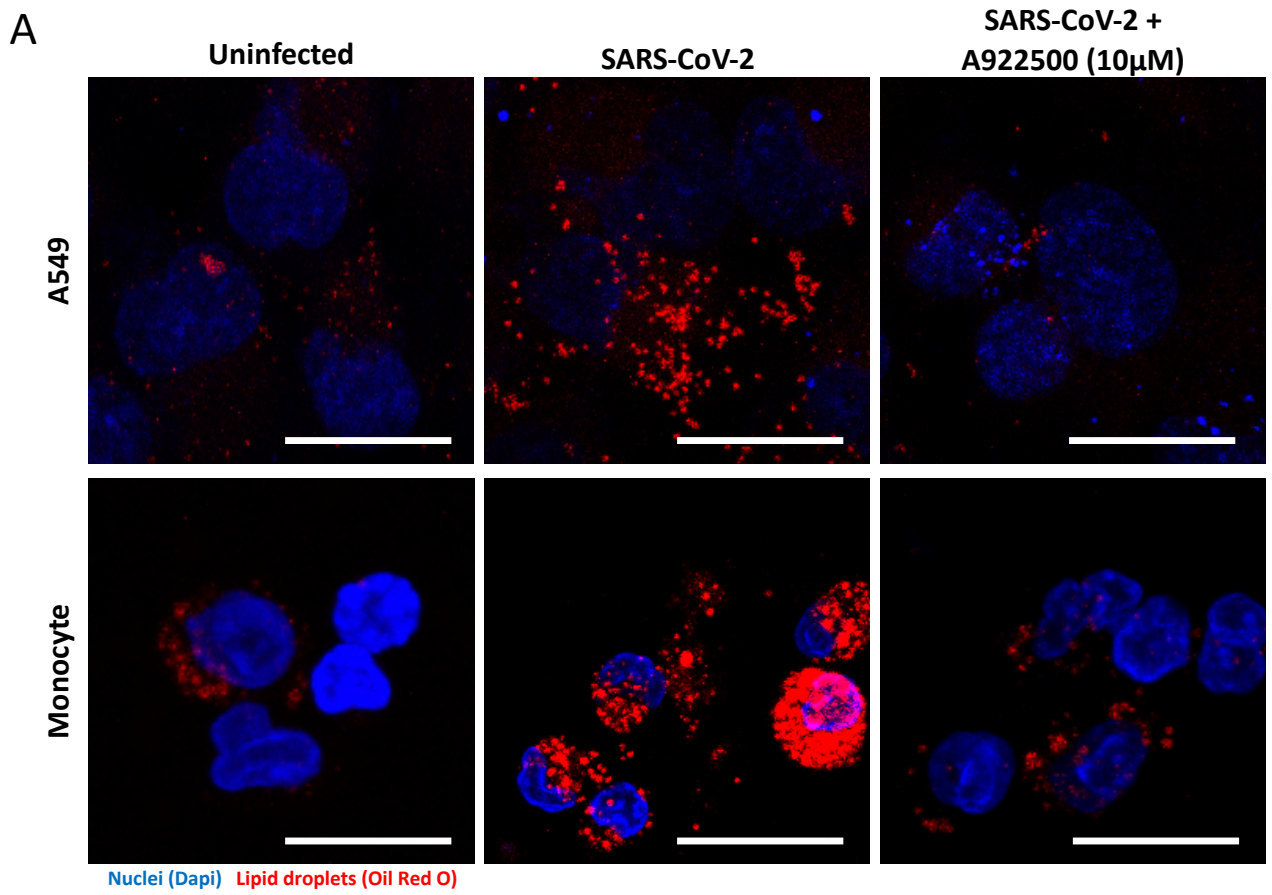
A
Uninfected
SARS-CoV-2
SARS-CoV-2 +
A922500 (10μM)
A549
Monocyte
Nuclei (Dapi)
Lipid droplets (Oil Red O)

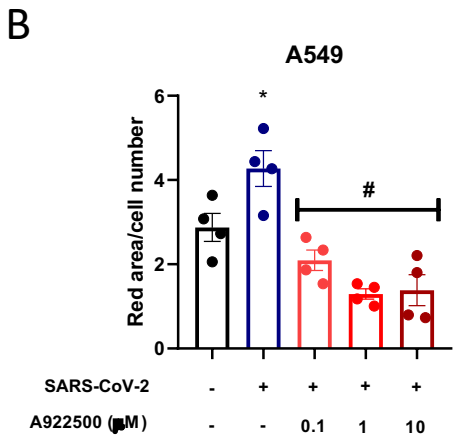
B
A549
Red area/cell number
SARS-CoV-2
A922500 (μM)

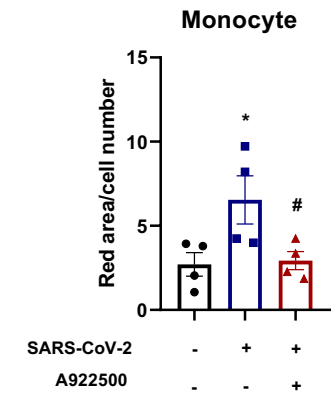
C
Monocyte
Red area/cell number
SARS-CoV-2
A922500

Figure 2

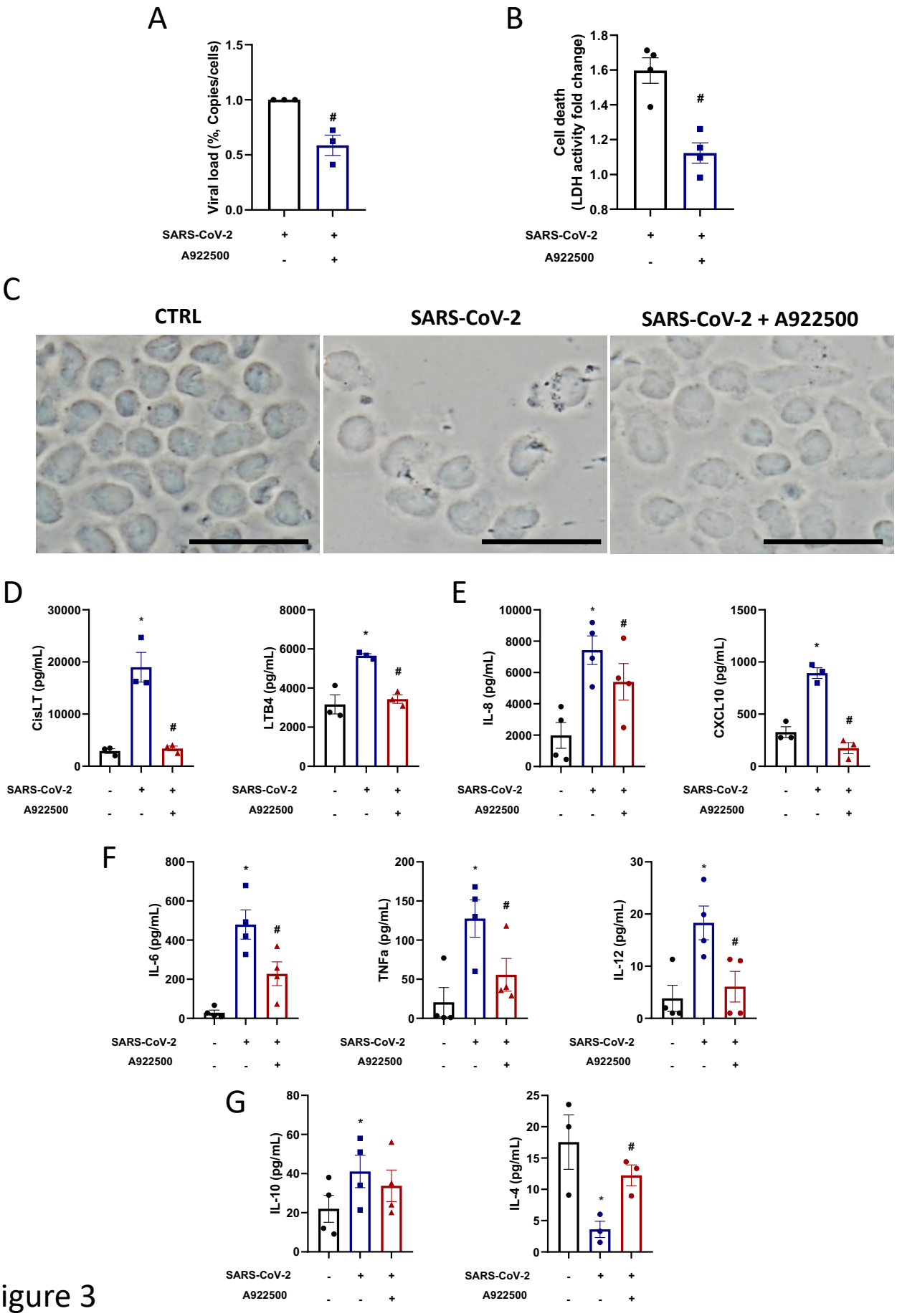
A
Viral load (%, Copies/cells)
1.5
1.0
0.5
0.0
#
SARS-CoV-2 + +
A922500 - +
B
Cell death
(LDH activity fold change)
1.8
1.6
1.4
1.2
1.0
0.8
#
SARS-CoV-2 + +
A922500 - +
C
CTRL
SARS-CoV-2
SARS-CoV-2 + A922500
D
CisLT (pg/mL)
30000
20000
10000
0
*
#
SARS-CoV-2 - + +
A922500 - - +
LTB4 (pg/mL)
8000
6000
4000
2000
0
*
#
SARS-CoV-2 - + +
A922500 - - +
E
IL-8 (pg/mL)
10000
8000
6000
4000
2000
0
*
#
SARS-CoV-2 - + +
A922500 - - +
CXCL10 (pg/mL)
1500
1000
500
0
*
#
SARS-CoV-2 - + +
A922500 - - +
F
IL-6 (pg/mL)
800
600
400
200
0
*
#
SARS-CoV-2 - + +
A922500 - - +
TNFa (pg/mL)
200
150
100
50
0
*
#
SARS-CoV-2 - + +
A922500 - - +
IL-12 (pg/mL)
30
20
10
0
*
#
SARS-CoV-2 - + +
A922500 - - +
G
IL-10 (pg/mL)
80
60
40
20
0
*
SARS-CoV-2 - + +
A922500 - - +
IL-4 (pg/mL)
25
20
15
10
5
0
*
#
SARS-CoV-2 - + +
A922500 - - +

Figure 3

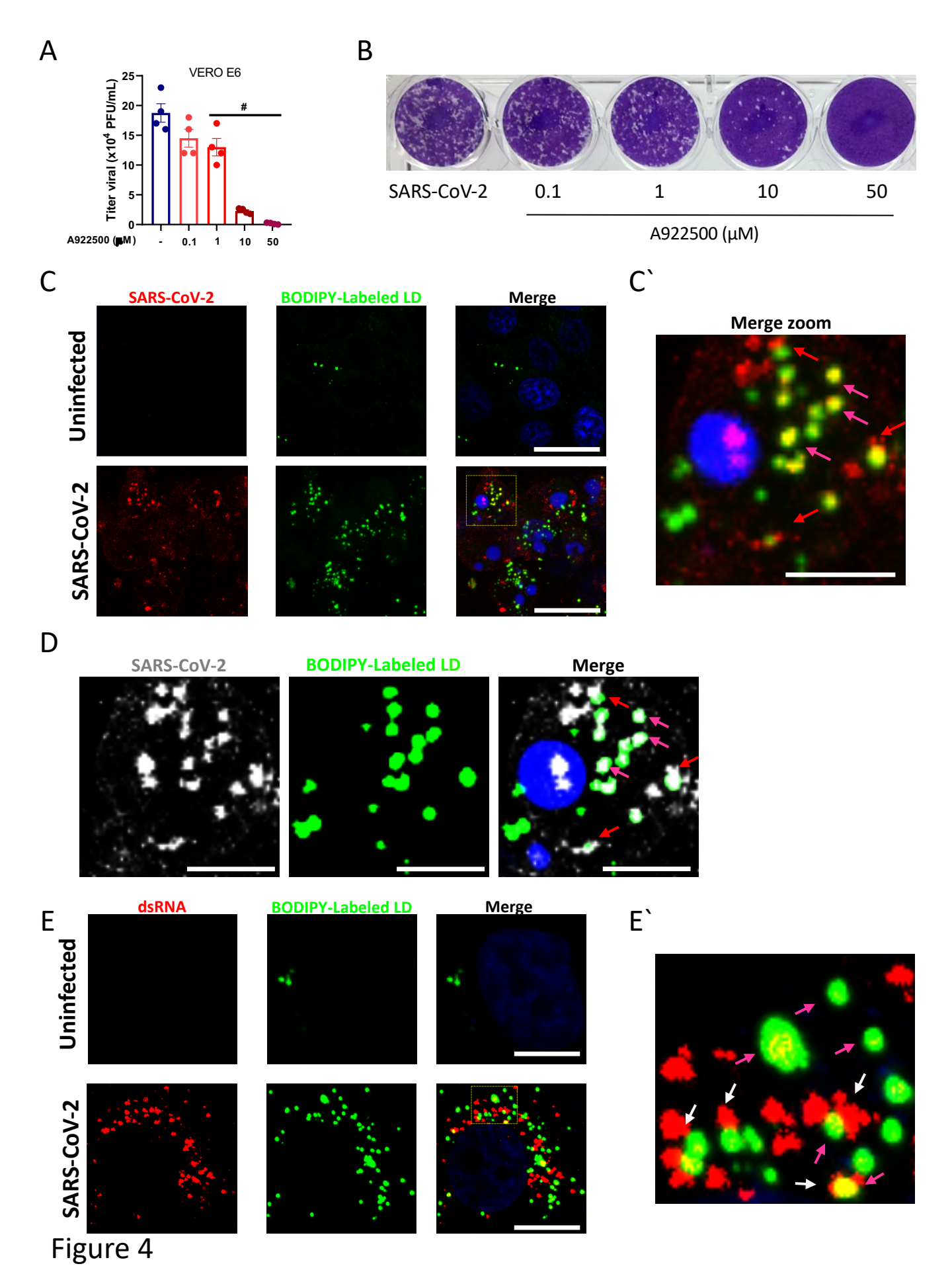
A
VERO E6
Titer viral (x10^4 PFU/mL)
25
20
15
10
5
0
#
A922500 (μM)
-
0.1
1
10
50
B
SARS-CoV-2
0.1
1
10
50
A922500 (μM)
C
SARS-CoV-2
BODIPY-Labeled LD
Merge
Uninfected
SARS-CoV-2
C`
Merge zoom
D
SARS-CoV-2
BODIPY-Labeled LD
Merge
E
dsRNA
BODIPY-Labeled LD
Merge
Uninfected
SARS-CoV-2
E`

Figure 4

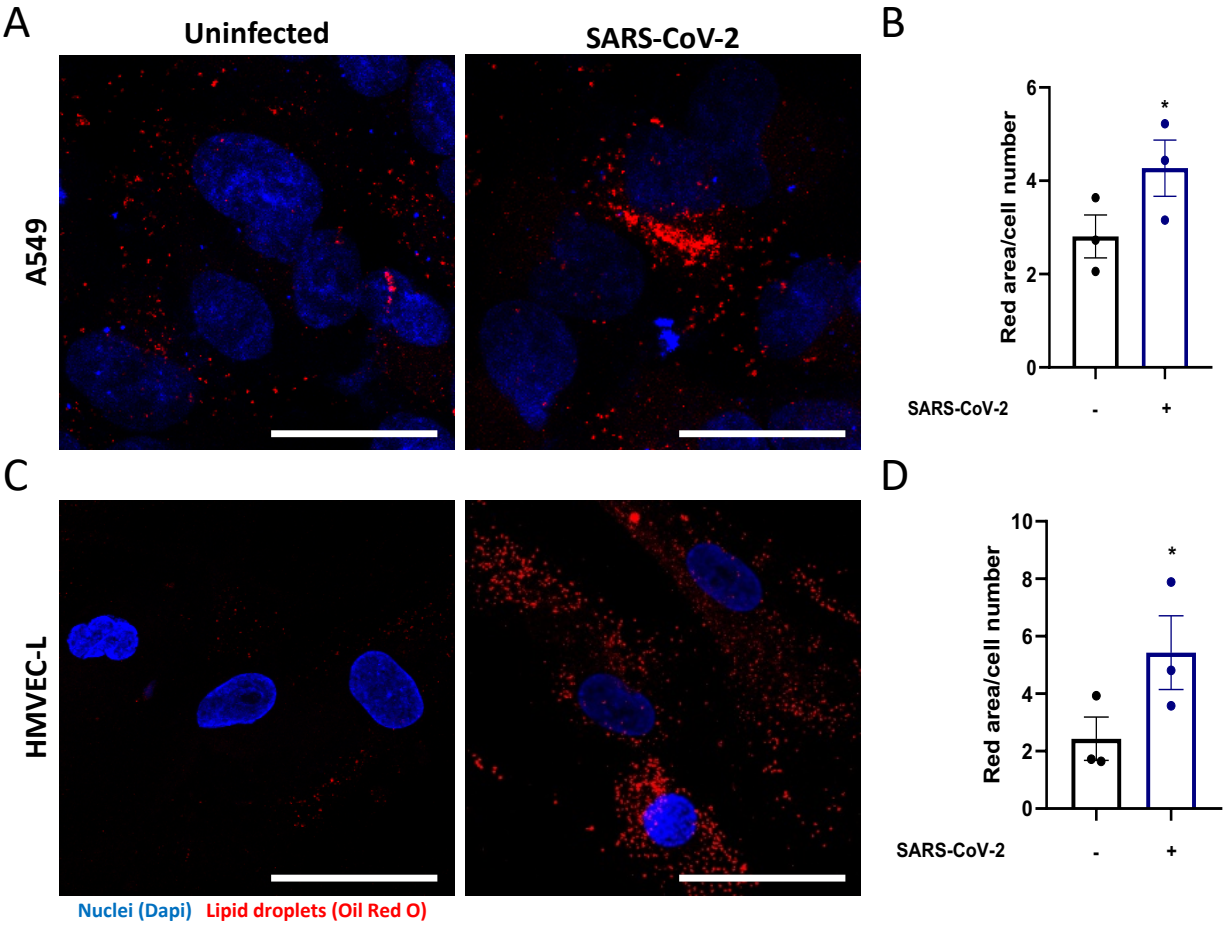

Supplementary Figure 1